applied optics

Visibly transparent organic photovoltaic with improved transparency and absorption based on tandem photonic crystal for greenhouse application

Fan Yang,[1] Ye Zhang,[1] Yuying Hao,[1,*] Yanxia Cui,[1] Wenyan Wang,[1] Ting Ji,[1] Fang Shi,[1] and Bin Wei[2]

[1]Key Lab of Advanced Transducers and Intelligent Control System of Ministry of Education, College of Physics and Optoelectronics, Taiyuan University of Technology, Taiyuan 030024, China
[2]Key Laboratory of Advanced Display and System Applications, Ministry of Education, Shanghai University, Yanchang Road 149, Shanghai 200072, China
[3]e-mail: yanxiacui@gmail.com
*Corresponding author: haoyuying@tyut.edu.cn

Received 28 August 2015; revised 4 November 2015; accepted 5 November 2015; posted 5 November 2015 (Doc. ID 248856); published 30 November 2015

We demonstrate a visible transparent organic photovoltaic (OPV) with improved transmission and absorption based on tandem photonic crystals (TPCs) for greenhouse applications. The proposed device has an average transmittance of 40.3% in the visible range of 400–700 nm and a high quality transparency spectrum for plant growth with a crop growth factor of 41.9%, considering the weight of the AM 1.5G solar spectrum. Compared with the corresponding transparent OPV without photonic crystals, an enhancement of 20.7% in the average transmittance and of 24.5% in the crop growth factor are achieved. Detailed investigations reveal that the improved transmittance is attributed to the excitation of the optical Tamm state and the light interference effect in TPC. Concomitantly, the total absorption efficiency in the active layer of the designed TPC based transparent OPV reaches 51.5%, being 1.78% higher than that of the transparent OPV without PC and 76% of that of the opaque counterpart. The improved absorption originates from the Bragg forbidden reflectance of TPC. Overall, our proposal achieves the optimized utilization of sunlight by light manipulation of TPC.

OCIS codes: (010.1030) Absorption; (050.5298) Photonic crystals; (160.4890) Organic materials; (350.6050) Solar energy.

http://dx.doi.org/10.1364/AO.54.010232

1. INTRODUCTION

As a renewable energy source technology, organic photovoltaics (OPVs) have drawn intense attention [1–3]. Of particular interest are the versatile functional applications utilizing their advantages of transparency, flexibility, light weight, low cost, and so on [4–10]. Up to now, the power-generating window based on visibly transparent OPVs has been actively developed for the demand of on-site electricity generation at surface areas of buildings [6–12], being not only economic but also environmentally friendly. However, the attempts made for applying OPVs in greenhouses [13,14] are quite few.

The growth conditions, including temperature, relative humidity, CO_2 concentration, ventilation, and so forth, are important factors influencing the yield and quality of greenhouse crops. The control of all these growth conditions often entails the consumption of electricity. On the other hand, a high crop yield requires a suitable light supply for efficient photosynthesis [15]. Therefore, it is better that the new generation of cellophane for greenhouses could generate the electricity and meanwhile optimize the light transmission spectrum. In detail, the cellophane should allow the photosynthetically relevant light to pass through and then to reach the plants, while harnessing the light unnecessary for the crop growth for electricity generation. The most promising scheme for realizing such a kind of cellophane is the visibly transparent OPV [13]. Besides of the functionalities of sharing the sunlight by plants and electricity generation, the OPV technology is compatible with the greenhouse application due to its advantage of flexibility. For such a specific application, a low bandgap active material is a prerequisite [16]. However, a low bandgap material does not directly guarantee high power conversion efficiency and optimal transmittance yet. Therefore, photonic management becomes very

essential to achieving ideal transparent OPVs suitable for the greenhouse application.

Recently, one-dimensional photonic crystals (1DPCs) have been used to tune the absorption and transmittance of transparent OPVs by taking advantage of the photonic bandgap [17–20]. The 1DPC as a Bragg reflector enables those photons with energies lying in the bandgap to be fed back into the device and then be captured twice or more efficiently, thereby increasing the light absorption. But the use of a single 1DPC would not synchronously produce the optimal light absorption and transmittance for the greenhouse application [17–20]. In this paper, we theoretically designed an easily-manufactured tandem photonic crystal (TPC)-based transparent OPV. The designed device demonstrates an average transmittance of 40.3% in the visible range of 400–700 nm and a high quality transparency spectrum for the crop growth with a defined crop growth factor [12] of 41.9%, corresponding to an enhancement of 20.7% in the average transmittance and of 24.5% in the crop growth factor compared to the transparent OPV without photonic crystals (PCs). Meanwhile, the average absorption efficiency in the active layer of our TPC-based transparent OPV reaches 51.5%, 1.78% higher than that of the transparent OPV without PC (50.6%) and 76% of that of the referred opaque OPV. The short-circuit current density of our TPC-based transparent OPV is 18.74 mA/cm^2, reaching 78% of that of its opaque counterpart. Our proposal is expected to provide theoretical guidance for applying transparent OPVs in greenhouses.

2. STRUCTURE AND METHOD

Figure 1(a) schematically presents the structure of the proposed TPC device (TPCD) based on a standard OPV of ITO/PEDOT:PSS/active layer/Ag. Here, 100 nm thick indium tin oxide (ITO) on a glass substrate is used as the transparent anode, followed by a 30 nm thick hole transport layer [poly(3,4-ethylenedioxythiophene):(polystyrene sulfonic acid, PEDOT:PSS]. Next, a 100 nm thick organic active layer (PDTP-DFBT:$PC_{71}BM$), consisting of poly[2,7-(5,5-bis-(3,7-dimethyloctyl)-5H-dithieno3, 2-b:2′, 3′-d] pyran)-alt-4,7-(5, 6-difluoro-2,1,3-benzothiadiazole) (PDTP-DFBT) (with very low bandgap and wide absorption spectrum [21]) and (6, 6)-phenyl-C71-butyric acid methyl ester] ($PC_{71}BM$), is placed on the PEDOT:PSS film. Subsequently, a 10 nm thick ultrathin Ag film is used as the cathode to make the device transparent [22]. Finally, the designed TPCs are deposited on the Ag cathode to manipulate light. Each PC of the TPCs consists of four layers of high refractive index material, TiO_2, alternately arranged with four layers of low refractive index material, LiF. For the bottom PC (i.e., PC1), the thicknesses of TiO_2 (t_1) and LiF (t_2) are 88 and 155 nm, respectively, and for the one sandwiched between the OPV and PC1 (i.e., PC2), the thicknesses of TiO_2 (t_3) and LiF (t_4) are 25 and 40 nm, respectively. The reason for the choice of PC1 and PC2 will be discussed later. The refractive indices of LiF and TiO_2 are experimentally measured without approximation, and the refractive indices of the PDTP-DFBT:$PC_{71}BM$ (1:2) blend are extracted from [21], as shown in Fig. 1(b). For comparison, two types of reference devices (RDs) without PCs are designed,

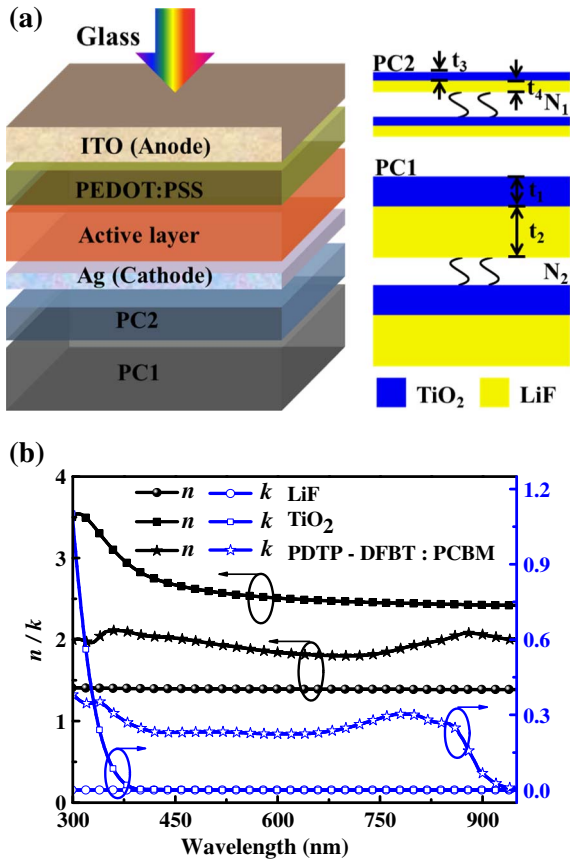

Fig. 1. (a) Schematic of the designed TPCD and cross-sectional view of the TPC. (b) Refractive indices of the materials used in the simulation.

termed as RD1 and RD2. RD1 is an opaque device with a 200 nm thick Ag film as the back electrode to block all transmission. RD2 is also a transparent OPV with completely the same OPV part as the TPCD. Additionally, another two transparent devices with only PC1 or PC2 are also designed as references, denoted as PC1D and PC2D, respectively. Their OPV parts are also identical with that of TPCD.

Throughout our simulations, all calculations were performed by the finite element method. Our numerical method has been verified by studying the problems in [23]. In practice, the thickness of the glass substrate (several millimeters) is much larger than that of the OPV part (a few hundred nanometers). In order to make our simulation model more close to reality, we simulate the situation of incident light entering into the device from a semi-infinite thick glass substrate rather than air, neglecting the transmission and reflection behaviors at the air–glass interface.

The absorptivity and transmittance at a specified wavelength, denoted by $A(\lambda)$ and $T(\lambda)$, can be directly extracted once the distribution of the electric field amplitude is calculated. Meanwhile, we also calculate another two essential parameters, namely, the average absorption and transmittance efficiency, denoted by A_{int} and T_{int}. In detail, $A_{\text{in}}t$ is obtained by integrating the absorptivity $A(\lambda)$ over the wavelength range of 350–900 nm to closely match the absorption band of the

active blend considering the weight of the AM 1.5G solar spectrum. Likewise, T_{int} is calculated by integrating $T(\lambda)$ over the wavelength range of 400–700 nm for matching the photosynthetically active radiation (PAR) [12–14], considering the weight of the AM 1.5G solar spectrum.

3. RESULTS AND DISCUSSION

To fully assess the transmittance capability and spectrum quality of the proposed TPCD and clearly grasp the impact of the TPCs, we examine the transmittance spectrum of the TPCD and compare it with those of the references. The wavelength-dependent transmittances of different devices at normal incidence are shown in Fig. 2(a), and the corresponding integrated transmittances are also shown in Table 1.

As summarized in Table 1, T_{int} of the TPCD reaches to 40.3%, increased by 20.7% and 24.3% relative to those of RD2 and PCD1, respectively. In detail, it can be seen from Fig. 2(a) that the transmittance of the TPCD is remarkably improved in the whole visible region in comparison with that of RD2. Compared to PC1D, the TPCD has higher transmittance, especially in the red light region, which is quite beneficial to the growth of plants as photosynthesis takes place at the red and blue band [24]. Though T_{int} of the TPCD is almost the same as that of PC2D, the merit of the TPCD is its better absorption property (as shown in Fig. 3). Besides, it is observed

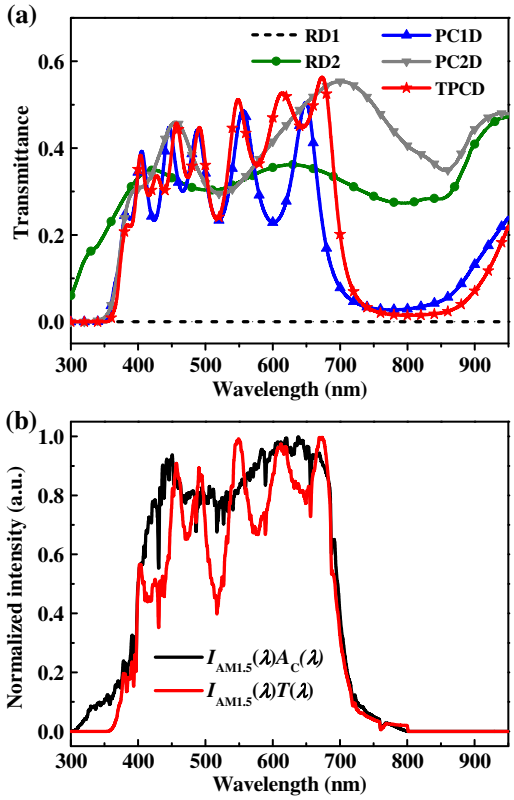

Fig. 2. (a) Transmittance spectra in different devices at normal incidence. Short dashed line: RD1; circles: RD2; upward triangles: PC1D; downward triangles: PC2D; and stars: TPCD. (b) Transmittance spectrum of TPCD and the relative action spectrum of plants considering the weight of the AM 1.5G solar spectrum.

Table 1. Summary of the Performance Parameters of Proposed and Reference Devices

Device	T_{int}	G	A_{int}	J_{sc} (mA/cm^2)	Q (mA/cm^2)
TPCD	0.4034	0.4186	0.5153	18.63	7.80
PC1D	0.3246	0.3107	0.5501	19.75	6.45
PC2D	0.4039	0.4088	0.4525	15.71	6.42
RD2	0.3341	0.3363	0.5063	17.94	6.03
RD1	0	0	0.6790	24.01	0

that the transmittance of the TPCD in the green light region (~520 nm) is a bit lower than that for PC2D while that in other light regions is a bit higher. This is another merit of the TPCD versus PC2D as green light contributes less to photosynthesis due to the poor light absorption of chlorophyll in this region [24]. It is also noticed that the transmittances in the ultraviolet (UV) region decrease to nearly zero for the TPCD and PCD1. This is what we expect because the UV radiation is very disadvantageous to the plant growth [25]. More intuitively, it can be seen from Fig. 2(b) that the profile of the transmittance spectrum of TPCD matches quite well with that of the plant action spectrum $A_c(\lambda)$ [12], which is obtained from the averaged absorption spectrum of 27 herbaceous plants [26]. In order to quantitatively evaluate the impact of transparent solar cells on plant growth, we calculated a crop growth factor G according to the following equation [12]:

$$G = \frac{\int_{400\ \mathrm{nm}}^{700\ \mathrm{nm}} T(\lambda) I_{\mathrm{AM1.5}}(\lambda) A_c(\lambda) \mathrm{d}\lambda}{\int_{400\ \mathrm{nm}}^{700\ \mathrm{nm}} I_{\mathrm{AM1.5}}(\lambda) A_c(\lambda) \mathrm{d}\lambda}. \quad (1)$$

Here, $I_{AM1.5}$ is the AM 1.5 solar spectral irradiance. The rate of photosynthesis in a crop is governed by the integral of the solar spectrum and the action spectra of plants, as seen in the denominator of Eq. (1). Therefore, the G factor represents the ratio of the rate of photosynthesis under an OPV cellophane and that under a clear sky. For TPCD, the G factor is equal to 41.9%, increased by 34.7%, 2.40%, and 24.5% compared with those of PC1D, PC2D, and RD2, respectively. It is well known that a 1% drop in photosynthesis will result in a 1% fall in crop production for most greenhouse crops [24]. From this

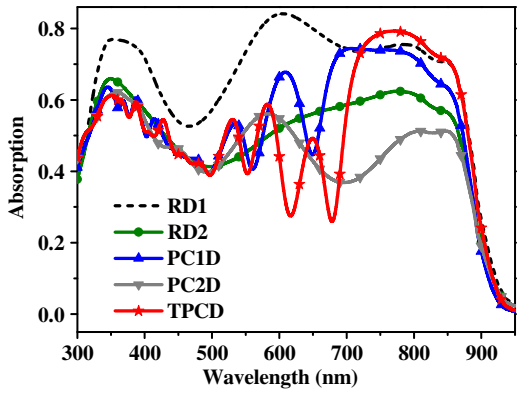

Fig. 3. Absorption spectra of active layers in different devices at normal incidence. Short dashed line: RD1; circles: RD2; upward triangles: PC1D; downward triangles: PC2D; and stars: TPCD.

point of view, our proposal is the most favorable device among all types of OPVs for the greenhouse application.

Next, we calculate the spectrally dependent absorption $A(\lambda)$ in the active layer part for different devices at normal incidence [23], as shown in Fig. 3. One can see clearly that the absorption efficiencies $A(\lambda)$ of the TPCD and PC1D are greatly enhanced in the 700–900 nm region compared with those of RD2 and PC2D due to the Bragg forbidden reflection of PC1. It is found that PC2 does not form any photonic bandgap in the considered wavelength range and thus makes PC2D exhibit lower absorption efficiency than RD2 [and in turn higher transmittance; see Fig. 2(a)]. To assess the total light absorption performance in the active layer, we calculate the average absorption efficiency A_{int}. A_{int} in the active layer of the TPCD is 51.5%, reaching 76% of that of the opaque RD1 and being 13.9% and 1.78% higher than those of PC2D and RD2, respectively, though 6.33% lower than that of PC1D (see Table 1).

It is well known that the short circuit current of a solar cell is proportional to the number of photons absorbed. In other words, the total absorption in the active layer for a solar cell determines the short-circuit current density (J_{sc}) of the whole device if the electrical losses are neglected. Consequently, the proposed device is assessed by its typical electrical performance parameter J_{sc}. Based on the obtained $A(\lambda)$, J_{sc} can be easily calculated by Eq. (2) [27]:

$$J_{\text{SC}} = e\int_{300\ \text{nm}}^{950\ \text{nm}} \text{IQE}(\lambda)\frac{\lambda}{hc}A(\lambda)I_{\text{AM1.5}}(\lambda)\text{d}\lambda, \tag{2}$$

where e is the charge of the electron, h is Planck's constant, c is the speed of light in a vacuum, and IQE(λ) is the internal quantum efficiency. The PC layers are used only for tuning the optical properties, and hence the electrical properties of the devices with PC are unchanged when they are added to the Ag cathode side. In our simulation models, since the active layer is thin enough, it is reasonable to assume that all absorbed photons are converted into collected charges [i.e., set IQE(λ) to 1], and based on that, the maximum value of J_{SC} (i.e., $J_{\text{SC-max}}$) is calculated. $J_{\text{SC-max}}$ for the TPCD is 18.63 mA/cm^2 and reaches up to 78% of that of the opaque RD1 [being close to the property level of the transparent OPV in [22], of which J_{sc} is 77% of that of the opaque cell]. In addition, $J_{\text{SC-max}}$ for the TPCD is 18.6% and 3.85% higher than those of PC1D and RD2, respectively, though 5.67% lower than that of PC2D (see Table 1).

To comprehensively evaluate the properties of transparent OPVs and distinguish the best device, we define a quality factor Q as follows:

$$Q = G \cdot J_{\text{SC}}. \tag{3}$$

The detailed results are shown in Table 1. One can see that the Q factor of the TPCD is the highest, increased by 20.9%, 21.5%, and 29.4% compared with PC1D, PC2D, and RD2, respectively. Therefore, our proposed device is the most optimal OPV for the greenhouse application, realizing the maximum utilization of sunlight.

In order to identify the underlying mechanisms of the improvement of transmittance and absorption in the proposed TPCD, the distribution map of the amplitude of the electric field ($|E|$) in the OPV is calculated; for comparison that of RD2 is also given, as shown in Figs. 4(a) and 4(b), respectively. Obviously, the electric field in the active layer of the TPCD is

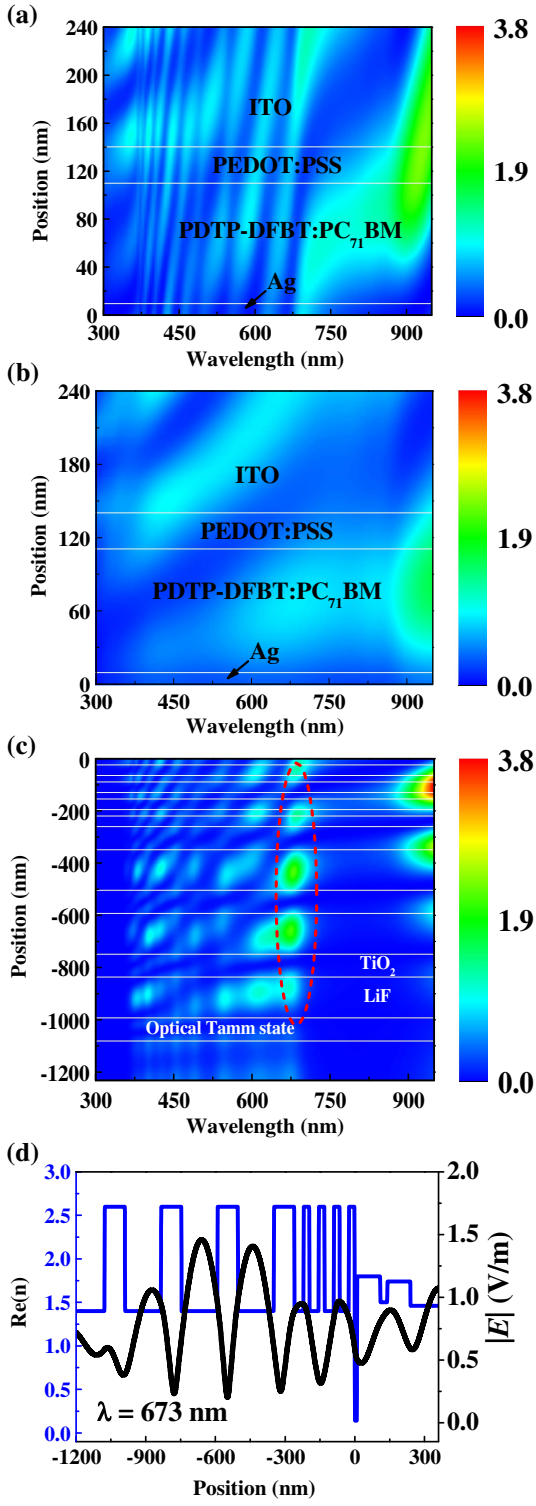

Fig. 4. Distribution maps of the amplitude of the electric field (a) in the OPV and (c) in the TPC for the TPCD and (b) that in the OPV for RD2 within the investigated wavelength band. (d) Profile of the amplitude of the electric field (black curve) and that of the real part of the refractive index (blue curve) at the Tamm resonance wavelength.

greatly strengthened in the wavelength range of 700–950 nm relative to that of RD2 due to the Bragg forbidden reflectance of PC1, in accordance with the enhanced absorption of the TPCD in the corresponding spectrum range (see Fig. 3). Figure 4(c) presents the distribution map of the amplitude of the electric field within the TPC layers of the TPCD alone, in which we observed the excitation of the optical Tamm state (OTS) at about 673 nm with the corresponding profile displayed in Fig. 4(d). Here, OTS, in analogy with the Tamm surface state, is a kind of interface mode supported between two different media, such as the metal/PC or the adjacent PCs. The critical feature of OTSs is that the field intensity is maximized at the interface and then decays gradually into the PC due to the Bragg forbidden band effect [28–32]. Different from the surface plasmon mode excited at the metal/dielectric interface, which can only be excited at the transverse-magnetic (TM) polarization, OTSs can exist under both TM and transverse-electric (TE) polarized light. Moreover, OTSs can be directly excited by free space incidence without the assistance of nanopatterned structures. In Fig. 4(d), it is observed that the OTS mode is formed at the heterojunction of PCs as the field profile exhibits oscillating-attenuation into PC1 and PC2 with the distance from the heterojunction. Therefore, the increased transmittance of the TPCD at the wavelength range of 600–700 nm is attributed to the resonant photon tunneling induced by OTS. In addition, Fig. 4(c) reflects that some bright spots also appear in the shorter wavelength range of 400–600 nm, but weaker than the OTS bright spots. These bright spots are formed due to light reflection back and forth in the PC multilayer film according to the interference theory. It is the formation of the interference mode that causes the selective transmittance within the TPCD in the wavelength range of 400–600 nm. Overall, the excitation of the OTS and the light interference effect induced by TPC are responsible for the improved transmittance of the TPCD.

To further study the influence of TPCs on the optical properties of device, the transmittance and reflection properties of PC1 alone and the PC1/PC2 combination on the Ag film (10 nm) are calculated. The incoming light enters into the structure from the Ag side. The number of PC bilayers is given by N_1 for PC1 and N_2 for PC2, and the reflectance and transmittance spectra of PC1/Ag and PC1/PC2/Ag films with different N_1 and N_2 are shown in Fig. 5.

It is found from Fig. 5(a) that for PC1/Ag, the reflectance increases sharply with the increase of N_1 at the wavelength range of 700–950 nm. PC1 with four cycles of bilayers already yields the reflectance at the photonic forbidden band approaching 100%, and no obvious increase is observed when N_1 is greater. In consideration of the cost, $N_1 = 4$ is selected. The corresponding transmittance shows the contrary law, as shown in Fig. 5(b). Afterward, the reflection and transmission properties of the PC1/PC2/Ag film with different N_2 are researched when fixing $N_1 = 4$. As described in Figs. 5(c) and 5(d), when $N_2 = 2$ or 6, the reflectance dip presents within the photonic forbidden bandgap of PC1, which is attributed to the excitation of OTSs at about 763 and 835 nm, respectively [see Figs. 6(a) and 6(c)]. This is negative for the absorption of light in the OPV. When $N_2 = 4$, the reflectance dip due to OTS is shifted to the edge of the photon forbidden band edge (~685 nm) as shown in Fig. 6(b). As a result, the photonic forbidden band of PC1 is maintained at the wavelength range

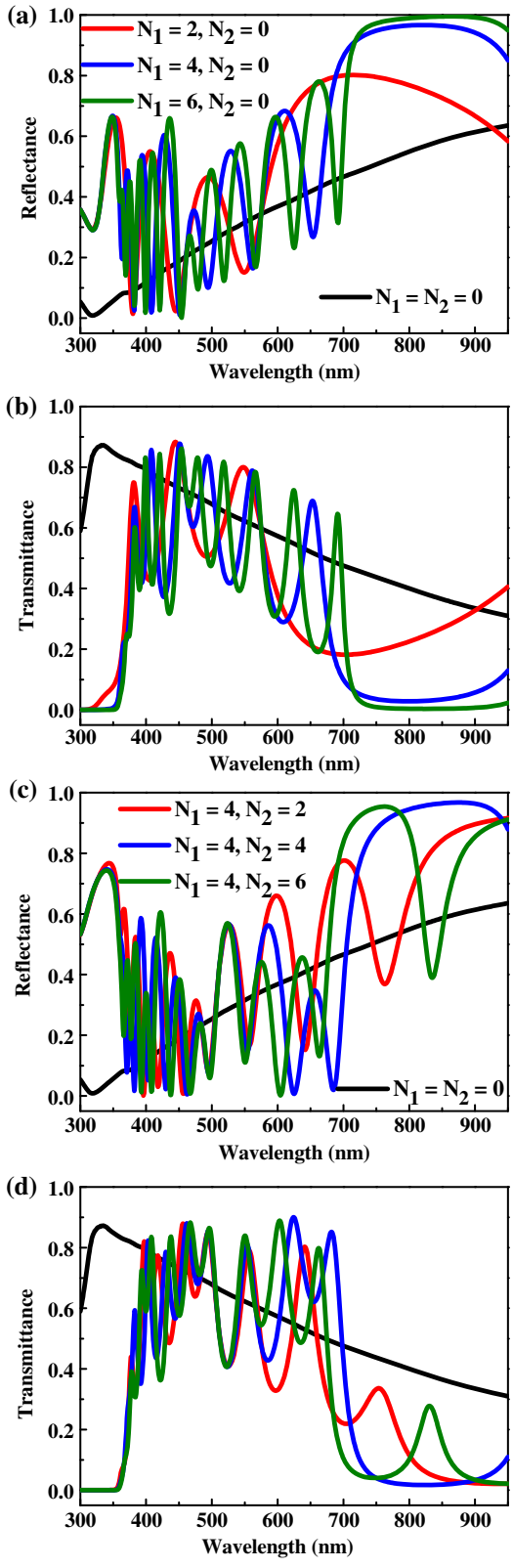

Fig. 5. (a) Reflectance and (b) transmittance spectra of PC1/Ag. (c) Reflectance and (d) transmittance spectra of PC1/PC2/Ag.

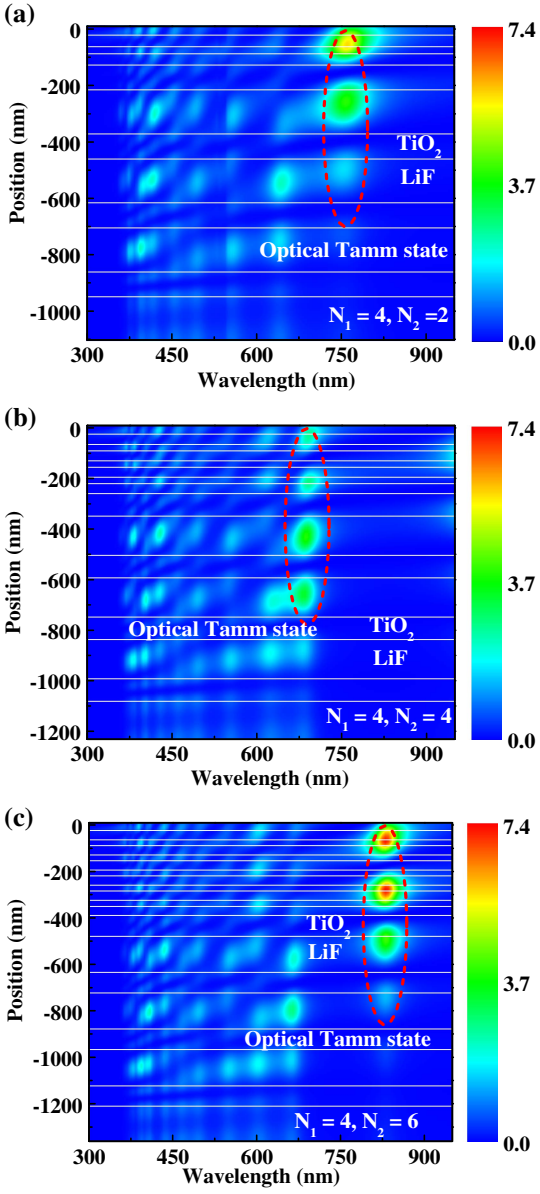

Fig. 6. Distribution maps of the amplitude of the electric field in different PC1/PC2/Ag structures within the investigated wavelength band. (a) $N_1 = 4$, $N_2 = 2$; (b) $N_1 = 4$, $N_2 = 4$; (c) $N_1 = 4$, $N_2 = 6$.

of 700–950 nm; thereby the high reflectance and low transmittance is achieved. Accordingly, $N_2 = 4$ is chosen in our proposal.

In the preceding investigation, only normally incident light incoming into the device is considered. In real operation, however, light often illuminates at varied directions. Therefore, it is important to explore the angular performance of the proposed transparent OPV for practical applications. Here, only the situation of incident light entering into the device from a semi-infinite thick glass layer is simulated. With consideration of the fact that the air–glass interface exists in reality, the incident angle from glass to the device is limited by the critical angle at the air–glass interface (~42 deg), which is set as the maximum

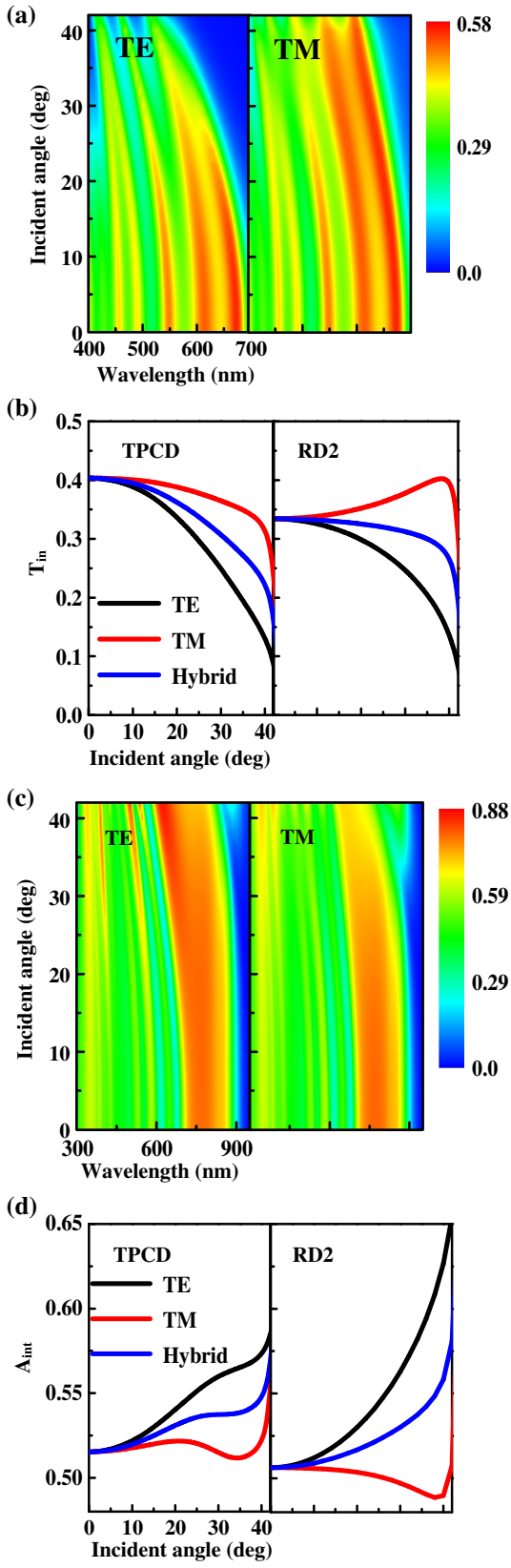

Fig. 7. Maps of the angular-dependent (a) transmission and (c) absorption as a function of wavelength for the TPCD at TE and TM polarization; (b) average transmission T_{int} and (d) absorption efficiency A_{int} versus the incident angle for TPCD and RD2 at different polarizations.

incident angle in the calculation. The transmission and absorption spectra versus the incident angle at TE and TM polarizations for the TPCD are depicted in Figs. 7(a) and 7(c).

It can be observed from Fig. 7(a) that the transmission is sensitive to the incident angle at both TE and TM polarizations for TPCD. The average transmission T_{int} of the TPCD rolls off with the increase of the incident angle at all polarizations [see Fig. 7(b), left panel]. For comparison, the angular-dependent T_{int} of RD2 at different polarizations is also plotted in Fig. 7(b) (right panel). When the incident angle increases to 40 deg, T_{int} at the hybrid polarization of the TPCD decreases to 22.5%, lower than that of RD2 (∼27.0%), but T_{int} of the TPCD remains higher than that of RD2 all the way up to 26 deg. It can be seen from Fig. 7(c) that the absorption is also sensitive to the incident angle at all polarizations, particularly at TE polarization. The corresponding average absorption efficiency at TE polarization increases remarkably as the incident angle increases, thereby leading to A_{int} increase at the hybrid polarization [see Fig. 7(d), left panel]. Again for comparison, the angular-dependent A_{int} of RD2 at different polarizations is also displayed in Fig. 7(d) (right panel). Figure 7(d) indicates that when the incident angle is smaller than 38 deg, A_{int} of the TPCD at the hybrid polarization is greater than that of RD2. In a word, our proposed device is more effective than RD2 at small incident angles, and thus it is more suitable for areas with long-time normally incident sunlight.

4. CONCLUSION

In conclusion, a visible transparent OPV with improved transmission and absorption based on TPC is put forward for greenhouse applications. Our study has demonstrated that the proposed device has an average transmittance of 40.3% in the visible range of 400–700 nm and a high-quality transparency spectrum with a crop growth factor of 41.9% considering the weight of the AM 1.5G solar spectrum. Compared with the transparent OPV without PC, enhancements of 20.7% in the average transmittance and of 24.5% in the crop growth factor have been achieved. The improved transmittance is attributed to the excitation of OTS and the light interference effect in the TPC. Meanwhile, the average absorption efficiency in the active layer reaches 51.5% considering the weight of the AM 1.5G solar spectrum, 1.78% higher compared than that of the corresponding transparent OPV without PC and 76% of that of the reference opaque OPV. The short circuit current density is 18.74 mA/cm^2, reaching 78% of that of its opaque counterpart. The improvement of absorption and the short circuit current density originate from the Bragg forbidden reflectance of TPC. In short, the proposed device can evidently increase the transmittance of photosynthetically relevant light and efficiently absorb light which is useless to crop growth for electrical generation, achieving the maximum utilization of sunlight. Our proposal is expected to provide theoretical guidance for applying transparent OPVs in greenhouse applications.

Funding. China Postdoctoral Science Foundation (2014M550152); Doctoral Program of Higher Education Research Fund (20121402120017); National Natural Science Foundation of China (NSFC) (11204202, 11204205, 21071108, 21101111, 61205179, 61274056); Outstanding Young Scholars of Shanxi Province, Hong Kong Scholar Program (XJ2013002).

REFERENCES

1. A. R. bin Mohd Yusoff, D. Kim, H. P. Kim, F. K. Shneider, W. J. da Silva, and J. Jang, "A high efficiency solution processed polymer inverted triple-junction solar cell exhibiting a power conversion efficiency of 11.83%," Energy Environ. Sci. **8**, 303–316 (2015).
2. L. Dou, J. You, J. Yang, C.-C. Chen, Y. He, S. Murase, T. Moriarty, K. Emery, G. Li, and Y. Yang, "Tandem polymer solar cells featuring a spectrally matched low-bandgap polymer," Nat. Photonics **6**, 180–185 (2012).
3. R. Søndergaard, M. Hösel, D. Angmo, T. T. Larsen-Olsen, and F. C. Krebs, "Roll-to-roll fabrication of polymer solar cells," Mater. Today **15** (1–2), 36–49 (2012).
4. S.-B. Kang, Y.-J. Noh, S.-I. Na, and H.-K. Kim, "Brush-painted flexible organic solar cells using highly transparent and flexible Ag nanowire network electrodes," Sol. Energy Mater. Sol. Cells **122**, 152–157 (2014).
5. W. Cao, Z. Li, Y. Yang, Y. Zheng, W. Yu, R. Afzal, and J. Xue, "'Solar tree': exploring new form factors of organic solar cells," Renewable Energy **72**, 134–139 (2014).
6. R. F. Bailey-Salzman, B. P. Rand, and S. R. Forrest, "Semitransparent organic photovoltaic cells," Appl. Phys. Lett. **88**, 233502 (2006).
7. J. Huang, G. Li, and Y. Yang, "A semi-transparent plastic solar cell fabricated by a lamination process," Adv. Mater. **20**, 415–419 (2008).
8. T. Ameri, G. Dennler, C. Waldauf, H. Azimi, A. Seemann, K. Forberich, J. Hauch, M. Scharber, K. Hingerl, and C. J. Brabec, "Fabrication, optical modeling, and color characterization of semitransparent bulk-heterojunction organic solar cells in an inverted structure," Adv. Funct. Mater. **20**, 1592–1598 (2010).
9. A. Colsmann, A. Puetz, A. Bauer, J. Hanisch, E. Ahlswede, and U. Lemmer, "Efficient semi-transparent organic solar cells with good transparency color perception and rendering properties," Adv. Energy Mater. **1**, 599–603 (2011).
10. C.-C. Chen, L. Dou, R. Zhu, C.-H. Chung, T.-B. Song, Y. B. Zheng, S. Hawks, G. Li, P. S. Weiss, and Y. Yang, "Visibly transparent polymer solar cells produced by solution processing," ACS Nano **6**, 7185–7190 (2012).
11. A. Henemann, "BIPV: built-in solar energy," Renewable Energy Focus **9**, 14–19 (2008).
12. Y. T. Chae, J. Kim, H. Park, and B. Shin, "Building energy performance evaluation of building integrated photovoltaic (BIPV) window with semi-transparent solar cells," Appl. Energy **129**, 217–227 (2014).
13. C. J. Emmott, J. A. Röhr, M. Campoy-Quiles, T. Kirchartz, A. Urbina, N. J. Ekins-Daukes, and J. Nelson, "Organic photovoltaic greenhouses: a unique application for semi-transparent PV?" Energy Environ. Sci. **8**, 1317–1328 (2015).
14. A. Yano, M. Onoe, and J. Nakata, "Prototype semi-transparent photovoltaic modules for greenhouse roof applications," Biosystems Eng. **122**, 62–73 (2014).
15. D. M. Gates, H. J. Keegan, J. C. Schleter, and V. R. Weidner, "Spectral properties of plants," Appl. Opt. **4**, 11–20 (1965).
16. L. Dou, W. H. Chang, J. Gao, C. C. Chen, J. You, and Y. Yang, "A selenium-substituted low-bandgap polymer with versatile photovoltaic applications," Adv. Mater. **25**, 825–831 (2013).
17. W. Yu, L. Shen, Y. Long, P. Shen, W. Guo, W. Chen, and S. Ruan, "Highly efficient and high transmittance semitransparent polymer solar cells with one-dimensional photonic crystals as distributed Bragg reflectors," Org. Electron. **15**, 470–477 (2014).
18. W. Yu, S. Ruan, Y. Long, L. Shen, W. Guo, and W. Chen, "Light harvesting enhancement toward low IPCE region of semitransparent polymer solar cells via one-dimensional photonic crystal reflectors," Sol. Energy Mater. Sol. Cells **127**, 27–32 (2014).
19. W. Yu, L. Shen, P. Shen, Y. Long, H. Sun, W. Chen, and S. Ruan, "Semitransparent polymer solar cells with 5% power conversion efficiency using photonic crystal reflector," ACS Appl. Mater. Interfaces **6**, 599–605 (2014).

20. D.-D. Zhang, X.-C. Jiang, R. Wang, H.-J. Xie, G.-F. Ma, Q.-D. Ou, Y.-L. Chen, Y.-Q. Li, and J.-X. Tang, "Enhanced performance of semitransparent inverted organic photovoltaic devices via a high reflector structure," ACS Appl. Mater. Interfaces **5**, 10185–10190 (2013).
21. L. Dou, C.-C. Chen, K. Yoshimura, K. Ohya, W.-H. Chang, J. Gao, Y. Liu, E. Richard, and Y. Yang, "Synthesis of 5 H-dithieno [3, 2-b: 2′, 3′-d] pyran as an electron-rich building block for donor-acceptor type low-bandgap polymers," Macromolecules **46**, 3384–3390 (2013).
22. R. Betancur, P. Romero-Gomez, A. Martinez-Otero, X. Elias, M. Maymó, and J. Martorell, "Transparent polymer solar cells employing a layered light-trapping architecture," Nat. Photonics **7**, 995–1000 (2013).
23. A. Abass, H. Shen, P. Bienstman, and B. Maes, "Angle insensitive enhancement of organic solar cells using metallic gratings," J. Appl. Phys. **109**, 023111 (2011).
24. H. P. Kläring and A. Krumbein, "The effect of constraining the intensity of solar radiation on the photosynthesis, growth, yield and product quality of tomato," J. Agron. Crop Sci. **199**, 351–359 (2013).
25. K. A. Hughes, B. Lawley, and K. K. Newsham, "Solar UV-B radiation inhibits the growth of Antarctic terrestrial fungi," Appl. Environ. Microbiol. **69**, 1488–1491 (2003).
26. K. Inada, "Action spectra for photosynthesis in higher plants," Plant Cell Physiol. **17**, 355–365 (1976).
27. L. Yang, L. Mo, Y. Okuno, and S. He, "Optimal design of ultra-broadband, omnidirectional, and polarization-insensitive amorphous silicon solar cells with a core-shell nanograting structure," Prog. Photovoltaics Res. Appl. **21**, 1077–1086 (2013).
28. X. Kang, W. Tan, Z. Wang, and H. Chen, "Optic Tamm states: the Bloch-wave-expansion method," Phys. Rev. A **79**, 043832 (2009).
29. A. Kavokin, I. Shelykh, and G. Malpuech, "Lossless interface modes at the boundary between two periodic dielectric structures," Phys. Rev. B **72**, 233102 (2005).
30. T. Goto, A. Dorofeenko, A. Merzlikin, A. Baryshev, A. Vinogradov, M. Inoue, A. Lisyansky, and A. Granovsky, "Optical Tamm states in one-dimensional magnetophotonic structures," Phys. Rev. Lett. **101**, 113902 (2008).
31. M. Kaliteevski, I. Iorsh, S. Brand, R. Abram, J. Chamberlain, A. Kavokin, and I. Shelykh, "Tamm plasmon-polaritons: possible electromagnetic states at the interface of a metal and a dielectric Bragg mirror," Phys. Rev. B **76**, 165415 (2007).
32. X.-L. Zhang, J.-F. Song, X.-B. Li, J. Feng, and H.-B. Sun, "Optical Tamm states enhanced broad-band absorption of organic solar cells," Appl. Phys. Lett. **101**, 243901 (2012).